LASER INTERFEROMETER GRAVITATIONAL WAVE OBSERVATORY
- LIGO -
CALIFORNIA INSTITUTE OF TECHNOLOGY
MASSACHUSETTS INSTITUTE OF TECHNOLOGY

Technical Note **LIGO-T2500320-v1** 09/26/2025

Magneto-Optical Trap Assembly for Cold Rubidium Quantum Filtering Applications

Talia E. Glinberg
Mentors: Daniel Grass and Dr. Lee McCuller

California Institute of Technology
LIGO Project, MS 18-34
Pasadena, CA 91125
Phone (626) 395-2129
Fax (626) 304-9834
E-mail: info@ligo.caltech.edu

Massachusetts Institute of Technology
LIGO Project, Room NW17-161
Cambridge, MA 02139
Phone (617) 253-4824
Fax (617) 253-7014
E-mail: info@ligo.mit.edu

LIGO Hanford Observatory
Route 10, Mile Marker 2
Richland, WA 99352
Phone (509) 372-8106
Fax (509) 372-8137
E-mail: info@ligo.caltech.edu

LIGO Livingston Observatory
19100 LIGO Lane
Livingston, LA 70754
Phone (225) 686-3100
Fax (225) 686-7189
E-mail: info@ligo.caltech.edu

http://www.ligo.caltech.edu/

1 Abstract

An innate filtering problem in GQuEST (Gravity from the Quantum Entanglement of Space Time) arises from shot noise in the projective readout of weak, high-frequency, stochastic space-time fluctuations that lie beyond LIGO's current sensitivity range. To address this, the RbQ project is developing a system that uses a 2D- and 3D-magneto-optical trap (MOT) setup to cool and trap rubidium atoms into atomic clouds that can be transported and used as tunable optical filters for enhanced signal detection. To drive the desired atomic transition in rubidium, 780 nm light was produced via second-harmonic generation in a waveguide, followed by alignment through a free-space and fiber-based optical setup. Laser frequency stabilization was achieved using the Pound-Drever-Hall locking technique, using a rubidium vapor cell as a frequency reference. This work advances the use of cold atom-based quantum filters in next generation gravitational wave detectors, enabling improved projective readout and more sensitive detection of low SNR, high-frequency, signals beyond LIGO's current range.

2 Introduction

Laser Interferometer Gravitational-Wave Observatory (LIGO) was designed to detect gravitational waves—fluctuations in spacetime predicted by Einstein's theory of general relativity. [1] These waves are typically generated by massive astrophysical events like black hole collisions and neutron star mergers. While the LIGO has successfully observed gravitational waves, the instruments—Michelson interferometers with 4km-long arms—are sensitive to signals at audio frequencies (kHz range) which are lower frequencies than those at which holographic quantum gravity is predicted to peak.

LIGO is limited by quantum noise, specifically radiation pressure noise and shot noise. Radiation pressure originates from tiny fluctuation in the mirrors when they are hit by photons. Shot noise arises from the Heisenberg uncertainty principle and the fundamental concept of particle-wave duality that describes the quantum nature of light. When a laser beam fires photons at a detector, it is not possible to precisely predict when each photon will arrive at the detector given that the position and momentum of each photon cannot be known simultaneously. The photons arrive randomly in time according to a Poissonian distribution. At higher intensities, a larger number of photons will arrive the detector at a given moment minimizing the uncertainty that arises from these random fluctuations. At lower intensities, fewer photons hitting the detector results in greater uncertainty and leads to shot noise which limits signal detection at high frequencies, thus LIGO being sensitive at audio frequencies.

Because of this limitation, the detection of quantum gravitational effects remains a challenge. The GQuEST (Gravity from the Quantum Entanglement of Space Time) experiment is expanding the search for quantum gravitational effects by using two ultra-sensitive collocated tabletop Michelson interferometers with 7 m-long arms—3 orders of magnitude smaller

than LIGO-and a superconducting nanowire single-photon detector rather than the standard homodyne readout scheme that LIGO currently implements. This novel photon counting detection scheme will circumvent quantum shot noise as the limiting noise source by using optical cavities to filter the output light from the interferometer so that individual photons from the carrier signal can be detected. [2] Eliminating quantum noise from the detection scheme results in classical noise from thermal excitations of the optics as the dominant noise source.

The RbQ experiment in the McCuller Lab aims to build enhanced tunable optical filters to enable the use of this novel photon counting readout scheme in GQuEST and eventually LIGO. This detection scheme will be used to enable the detection of stochastic, low SNR, high-frequency, signals that lie outside of LIGO's current range. The objective of the RbQ project is to use cooled and trapped Rubidium-87 (^{87}Rb) atoms in conjunction with optical cavities to make improved filters with applications for holographic quantum gravity searches and neutron star mergers. [3] These cold atom quantum memory systems will lead to high-resolution spectral filtering by enabling multiplexing and acting as selective absorbers of specific frequencies of light.

3 Background

Atoms at room temperature move at high velocities, making it difficult to precisely manipulate or observe them. However, using laser cooling and trapping, their motion can be drastically reduced, enabling precise control over atomic position and momentum. This is especially useful in experiments that involve manipulation and observation of quantum phenomena, such as those conducted by the RbQ, GQuEST, and LIGO projects. One of the most common and effective cooling mechanisms is the magneto-optical trap (MOT). In a MOT, atoms in motion are slowed down by radiation pressure from red-detuned, circularly polarized light. Each time an atom absorbs a photon, it recoils as a result of the conservation of momentum, which slows and cools it, a process known as Doppler cooling. The force from the detuned laser driving a transition from the ground state $|g\rangle$ to the excited state $|e\rangle$ is written as:

$$\vec{F}_{\pm} = \pm\frac{\hbar\vec{k}\Gamma}{2}\frac{s_0}{1+s_0+(2\delta_{\pm}/\Gamma)^2} \tag{1}$$

Where $\hbar$ is Planck's constant divided by 2π, $\vec{k}$ is the wavevector that describes the direction and magnitude of the wave propagation, Γ is the scattering rate, $\delta_{\pm} = \delta \mp kv \pm g\mu_B B'z/\hbar$ is the detuning from the atom's frame of reference, and g is the g factor. The saturation parameter s_0 is defined as

$$s_0 = \frac{2|\Omega|^2}{\Gamma^2} \tag{2}$$

and is proportional to the intensity through the Rabi frequency Ω by $|\Omega|^2 \propto I$. [4].

3.1 Second-Harmonic Generation

In the process of second-harmonic generation (SHG), an input beam with frequency ω produces a beam with an output frequency of 2ω by passing through and interacting with a material with second order nonlinear optical susceptibility, denoted as $\chi^{(2)}$.

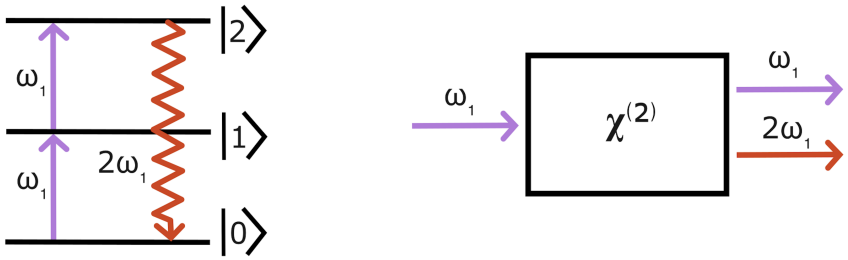

Figure 1: SHG energy-level diagram and schematic representation

SHG is a nonlinear process, which means that the response of the material is not proportional to the applied electric field, which can be written as

$$E(t) = E_0 \cos(\omega t) \tag{3}$$

and the nonlinear polarization is expressed as

$$P(t) = \epsilon_0[\chi^{(1)}E(t) + \chi^{(2)}E^2(t)] \tag{4}$$

$$P(t) = \epsilon_0[\chi^{(1)}E_0 \cos(\omega t) + \chi^{(2)}{E_0}^2 \cos^2(\omega t)] \tag{5}$$

$$P(t) = \epsilon_0[\chi^{(1)}E_0 \cos(\omega t) + \chi^{(2)}{E_0}^2(\frac{1}{2}(1 + \cos(2\omega t)) \tag{6}$$

where ϵ_0 is the permittivity of free space, $\chi^{(1)}$ is the first order linear susceptibility and $\chi^{(2)}$ is the second-order nonlinear susceptibility. The input frequency ω comes from the linear response in the first term and the doubled frequency 2ω is generated by the nonlinear response in the second term of Equation 6. If properly executed under optimal conditions, SHG can be so efficient that almost all the power from the incident laser (at frequency ω) will be frequency doubled. [5]

SHG can be achieved either through fiber-based methods or in free space. In fiber-based SHG, a nonlinear crystal is integrated into an optical fiber. This method has increased conversion efficiency and does not require extensive alignment once set up. In free-space SHG, a bulk nonlinear crystal with second order nonlinear optical susceptibility is placed in the path of a laser beam at the waist. This method requires precise alignment of the beam waist size, location, and angle to achieve maximum coupling efficiency. Free-space waveguides are quite difficult to align but a major advantage this method offers is the ability to use both the frequency doubled light as well as the output of light with the original frequency.

3.2 Pound Drever Hall Locking

The Pound–Drever–Hall (PDH) frequency stabilization technique was used to lock the laser and prevent frequency drifting. The phase of the laser is modulated using an electro-optic modulator (EOM). This modulation creates sidebands above and below the resonant carrier signal. These PDH sidebands do not interact with the frequency reference, so only the reflected beam mixes with the modulation signal. A feedback loop then uses the resulting error signal to correct the laser frequency and keep it locked.

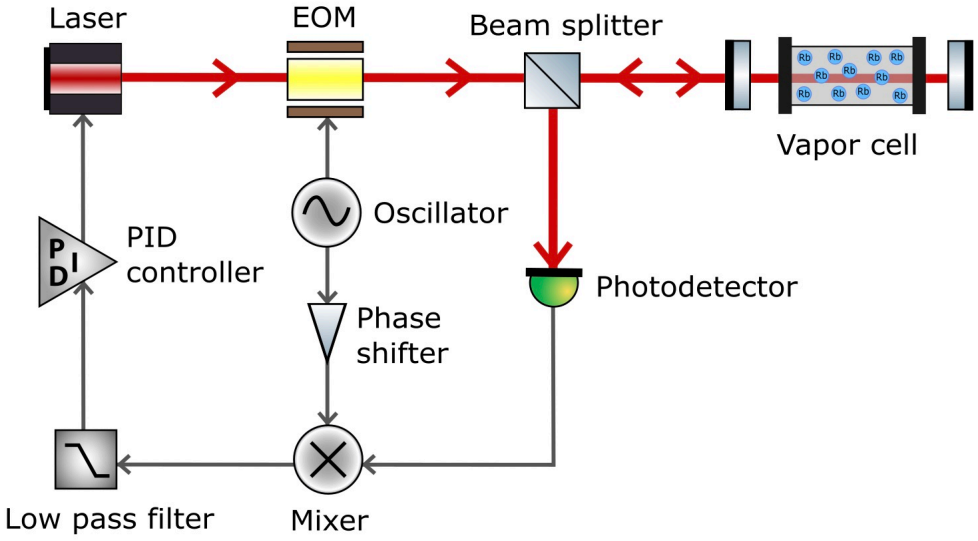

Figure 2: PDH locking feedback loop schematic

PDH locking can be done using an optical cavity as a frequency reference or by locking the laser directly to an atomic transition in a vapor cell. For this project, a vapor cell containing ^{87}Rb atoms was used as the reference. Using an atomic transition has the advantage that it is an absolute frequency reference, meaning the D2 atomic transition of ^{87}Rb at 780.24 nm is a fixed physical constant that does not drift over time. In contrast, optical cavities are relative references, since their resonance frequencies depend on external factors such as cavity length and temperature.

Since this experiment requires resonance with the ^{87}Rb D2 atomic transition for cooling and trapping in the MOT, the vapor cell provides a straightforward and reliable way to frequency lock the laser. The PDH locking technique is particularly useful because the error signal that is produced is directional: the sign of the signal indicates whether the laser frequency is above or below resonance, not just how far off it is. This allows the feedback loop to continuously readjust and push the laser in the correct direction.

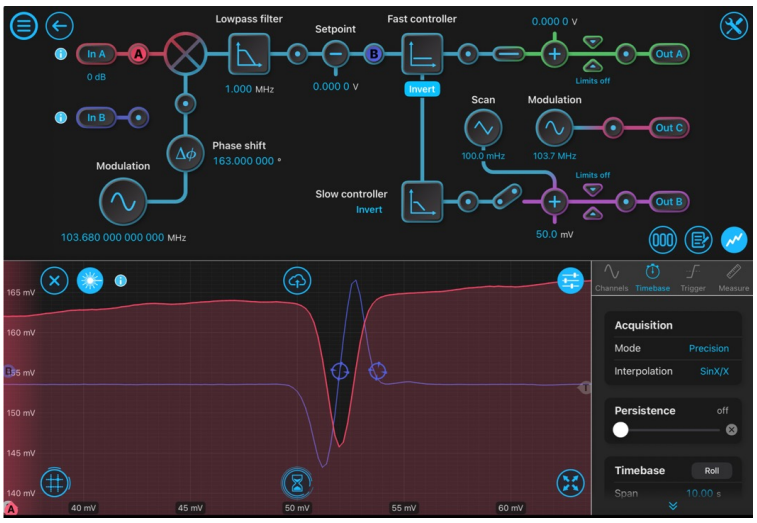

Figure 3: Absorption dip (red) and error signal (blue)

3.3 Tuning Laser Wavelength

To lock the 1560 nm laser, the beat note technique was used to match the laser frequency to the ^{87}Rb atomic transition. Direct wavelength measurements are not sufficient because wavemeters typically provide only MHz–GHz accuracy, and locking to an atomic transition requires much finer precision. The beat note method allows the frequency difference between the two lasers to be measured more precisely. A beat note is an interference pattern produced when two lasers with slightly different frequencies are overlapped in space. If the beams are aligned both spatially and in polarization (and not orthogonal), the interference generates an oscillating signal at the frequency difference of the two lasers [6]. This beat frequency can then be detected using a photodetector with an appropriate bandwidth and used to determine the frequency difference between the two lasers.

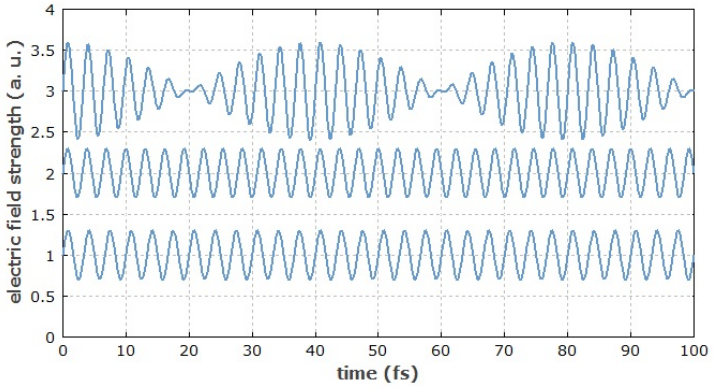

Figure 4: Beat note interference pattern [6]

The wavelength resonant to the D2 transition of ^{87}Rb is 780.24 nm in vacuum [7]. A weaker 780 nm laser was already tuned to this transition, so it was used as the reference to lock the 1560 nm laser. The original plan was to scan the 1560 nm laser's wavelength until a beat note with the 780 nm laser appeared. This proved technically challenging due to the steps

needed to make small adjustments to the 1560 nm laser's wavelength. Instead the 780 nm laser was used to scan until the two lasers were close enough that the beat note fell within the detector's bandwidth. From there, it was possible to iteratively tune both lasers until the 1560 nm laser was locked to the desired transition.

3.4 Magneto-Optical Traps

In this experiment, a 2D and a 3D magneto-optical trap (MOT) were implemented to create the cold, trapped, atomic clouds. The 2D MOT is the ^{87}Rb source—it fires stream of Rb atoms into 3D MOT. It produces a Rb beam using two orthogonal laser beams inside the MOT. This cools the atoms in the X and Y direction while pushing them out of the 2D MOT to the 3D MOT using a beam in the Z direction. Magnetic coils are used to induce a magnetic field gradient which enables trapping in the X-Y plane. The cooling and trapping mechanisms are how the 2D MOT is able to produce a cold atom flux of greater than 10^9 atoms per second [8]. There are many factors that influence the efficiency of the 2D MOT and whether or not it functions in general. These include laser power, wavelength, and light polarization. The 2D MOT fires a steady stream of ^{87}Rb into the 3D MOT, which is composed of a vacuum chamber, magnetic coils, as well as various optics and electronics. The 3D MOT is where the cold, dense, atomic clouds are formed and trapped. Cooling and trapping happen together but to understand how they work in conjunction, it is important to understand the individual mechanisms.

For laser cooling, there are three orthogonal laser beams as shown below in Figure 5, that are circularly polarized and slightly red-detuned from the D2 ^{87}Rb atomic transition.

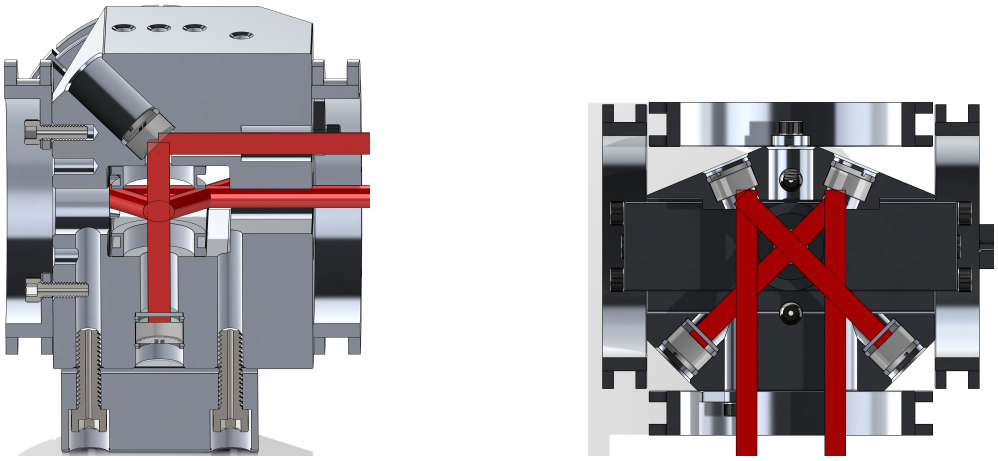

(a) Side view of 3D MOT (b) Top view of 3D MOT

Figure 5: Internal 3D MOT optics and beam path

Because the light is red-detuned, atoms in motion perceive the laser light as Doppler-shifted closer to resonance. Atoms moving toward a beam preferentially absorb photons which creates a radiation pressure force opposite their motion. Repeated cycles of absorption and spontaneous emission reduce the atoms' velocities. This is called Doppler cooling. At the

same time, a spatially varying magnetic field ($\vec{B}(\vec{r})$) is applied which shifts the atomic energy levels via the Zeeman effect which occurs due to the orbital and spin magnetic moments ($\vec{\mu}$) of electrons and is written as:

$$H = \vec{\mu} \cdot \vec{B}(\vec{r}) \tag{7}$$

Where H is the sum of the unperturbed Hamiltonian of the atom and the perturbation caused by the magnetic field. This spatially varying magnetic field produces a quadrupole magnetic field gradient that traps the atoms at the center of the MOT. The combination of cooling and trapping ensures that atoms moving away from the center of the trap always scatter more photons from the beam pushing them back toward the center. Together the red-detuned light slows the atoms and the magnetic field gradient provides a restoring force confining the atoms in three dimensions.

To operate a MOT effectively in the RbQ experiment, the atom begins in the singlet $S_{1/2}$ F=2 state and is excited to the triplet $P_{3/2}$ F'=3 state.

$$\text{ground state: } |5^2S_{1/2}; F = 2\rangle$$

$$\text{excited state: } |5^2P_{3/2}; F' = 3\rangle$$

$$\text{dark state: } |5^2S_{1/2}; F = 1\rangle$$

The total angular momentum $\vec{F}$ is a sum of the orbital angular momentum $\vec{L}$, the electron spin $\vec{S}$, and the nuclear spin $\vec{I}$ (with a magnitude of $\frac{3}{2}$ for ^{87}Rb). These differing total angular momentum values are hyperfine states within each electronic energy level. The cycling of this resonant transition is essential for trapping, although off-resonant excitation to the F'=2 state can occur as well. Using circularly polarized light helps minimize this by enforcing selection rules ($\Delta m_F = \pm 1$) that drive transitions to return the atoms to the original ground state. This reduces the probability of populating dark states.

If atoms are excited to the F'=2 state, they can decay to the $S_{1/2}$ F=1 dark state and this transition does not interact with the cooling laser. To prevent atoms from accumulating in the dark state, a repump laser is used to excite the atoms from F=1 back to F'=2, from which they can decay to F=2 and reenter the main MOT transition cycle.

4 Methods

4.1 Waveguide

For this project, a free-space waveguide was used for SHG to double the frequency of light from a 1560 nm laser to obtain 780 nm light—the frequency that excites the ^{87}Rb transition required to operate the magneto-optical trap (MOT). To achieve this, the 1560 nm laser beam was passed through the various optical components that are shown below in Figure 6, including half waveplates, a Faraday isolator and an aspherical focusing lens.

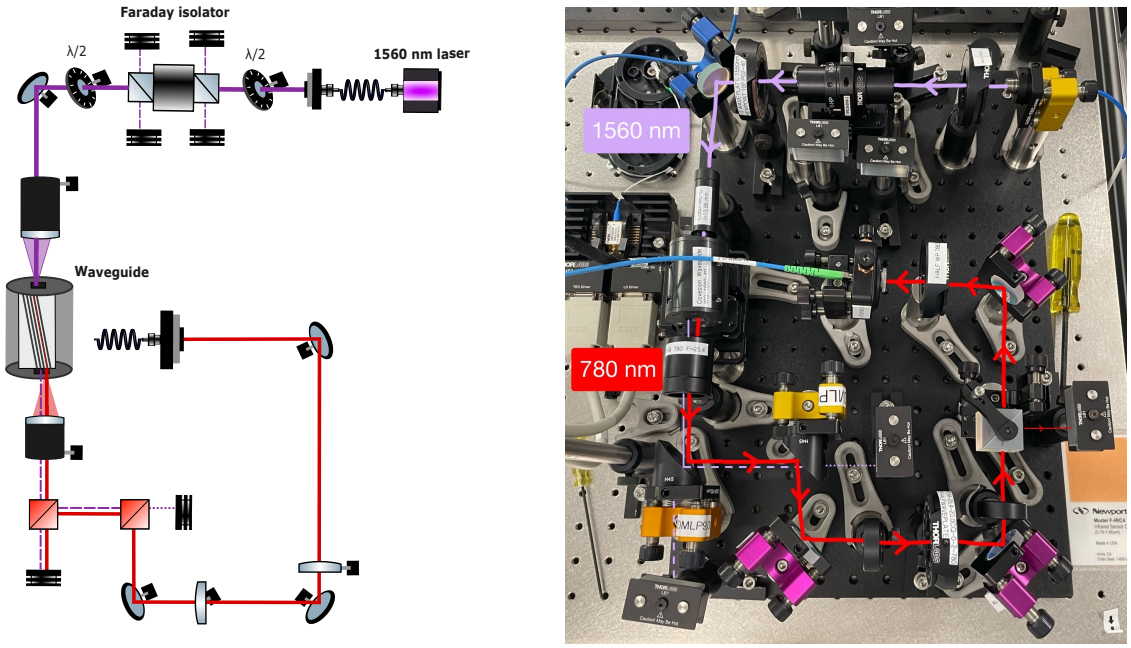

(a) SHG beam path schematic

(b) SHG optics and beam path

Figure 6: Schematic representation of the beam path and experimental setup of SHG optical components

The half waveplates are used to control polarization and the Faraday isolator prevents back-reflection from reaching the laser. These components were used to make the radius of beam waist 4.6 µm, small enough to fit into the waveguide. There is a magnesium doped lithium niobate crystal in the waveguide which has second order nonlinear susceptibility as well as a zinc planar layer that has ridges that define the waveguide grooves that the beam couples into. For efficient SHG, a gaussian beam shape is required and must be mode-matched to the waveguide's lowest-order mode. If the beam waist is too large or too small, or if there is significant astigmatism, the coupling efficiency drops and higher-order modes are excited. These modes are much less efficient or do not contribute to SHG at all.

The first part of the alignment process was adjusting the beam's waist size and location by carefully placing the aspherical lens using a beam profiler. This ensures the beam is small enough and correctly positioned to couple into the waveguide with minimal loss and maximum mode overlap. The waveguide itself is mounted on a 5-axis stage that allows precise control over the beam alignment in five spatial degrees of freedom: x (beam propagation direction), y, z, pitch, and yaw. Aligning the laser through the waveguide involved extensive scanning through various position by adjusting these five degrees of freedom in very small increments while monitoring the 780 nm output on a camera that is insensitive to the 1560 nm light.

In addition to spatial alignment, polarization and temperature must also be carefully controlled. The waveguide is polarization-sensitive and therefore requires precise adjustment of the half-wave plate before the waveguide. Temperature tuning is also essential to achieve

optimal mode matching. Overall, successful SHG using a waveguide requires optimizing the beam shape, spacial alignment using the 5 axis stage as well as the mirror positioned before the aspherical lens, polarization, and crystal temperature. The alignment and power maximization process involves iterative tuning to achieve strong, stable 780 nm output.

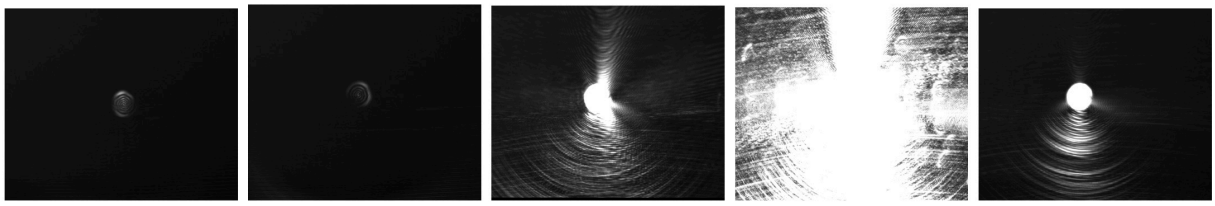

(a) groove 1 (b) groove 2 (c) groove 3 (d) groove 4 (e) groove 5

Figure 7: 780 nm light output after aligning the 1560 nm beam through each of the 5 grooves in the SHG crystal

4.2 Frequency Locking with a Vapor Cell

Once the laser was aligned and coupled to the lowest-order mode of the SHG crystal, 780 nm light was produced and coupled into an fiber optic cable and directed to the ^{87}Rb vapor cell setup used for PDH locking. The beam was divided by a beamsplitter into a strong pump beam and a weaker probe beam. These two beams were aligned so that they were counter-propagating through the ^{87}Rb vapor cell. To make sure the beams were spatially overlapping in the vapor cell, each beam was profiled to determine the waist size and location. These values were used to create a model in JAMMT software to determine appropriate lens focal lengths and positions for mode matching. This mode matching procedure ensured that the pump and probe beams were spatially overlapped with the desired waist size at the location of the vapor cell. Figure **??** shows the geometry of the pump and probe beam paths in the experimental setup.

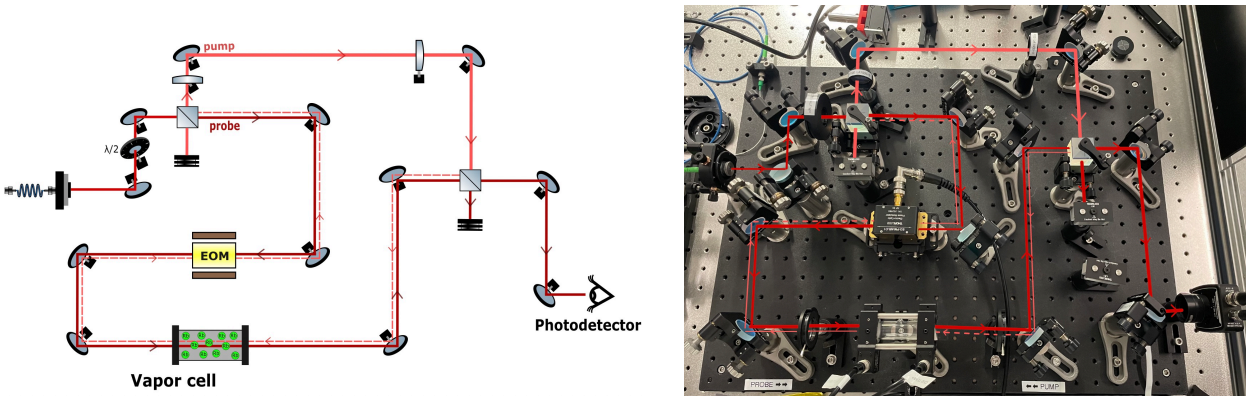

(a) PDH beam path schematic (b) PDH optics and beam path

Figure 8: Schematic representation of the beam path and experimental setup of optical components used for PDH locking

The counter-propagating pump–probe configuration enables saturated absorption spectroscopy (SAS). When a single laser beam interacts with the ^{87}Rb atoms in the vapor cell, the dip observed in the absorption spectrum is broad due to the Doppler effect. Atoms in the vapor move at different speeds. From the frame of reference of atoms moving toward the laser, the frequency of the light is blue-shifted; for atoms moving away from the laser, the frequency of the light is red-shifted. This results in the atoms moving in different speeds to be resonant at different frequencies which leads to an absorption dip that is much broader than the desired atomic transition. SAS addresses this issue by using counter-propagating beams in a pump–probe geometry. The signal from the weaker probe beam is detected using a photodetector, while the function of the strong pump beam is to control the population of atoms. Atoms in motion interact resonantly with only one beam at a time because the Doppler shifts for the counter-propagating beams are in opposite directions. Only atoms with zero velocity along the beam see both beams at exactly the same frequency. When the laser frequency is on resonance with the true atomic transition, atoms with zero velocity absorb strongly from the pump beam. The strong pump beam saturates this atomic population, meaning the atoms are excited faster than they can relax back to their ground state and as a result, they absorb fewer additional photons from the counter-propagating probe beam. As the laser scans across the atomic transition frequency, atoms exactly on resonance are saturated by the pump so the probe absorption dips sharply and this feature is visible on top of the Doppler-broadened background peak. These sharp dips provide a more precise frequency reference, allowing for more effective laser stabilization.

4.3 Fiber Connections

To deliver the right amount of power to the 2D MOT and the 3D MOT, the 780 nm light output from the SHG was filtered using dichroics and then coupled in to a patch fiber optic cable. This cable was connected to a series of fibers, including multiple fiber beam splitters and a fiber electro-optic modulator (EOM). The distribution of power to the PDH locking setup and the MOTs is shown in Figure 9.

A lot of work and troubleshooting was required to minimize losses in the fiber network. The main culprit was the fiber mating sleeves that are used to connect fiber patch cables, fiber beamsplitters, and the fiber EOM. The orientation of the fiber in the mating key played a large role in the efficiency so to mitigate power loss caused by improper orientation, narrow-key mating sleeves were purchased and implemented to replace the wide-key mating sleeves.

Another significant challenge was the unintentional formation of of a Mach-Zehnder interferometer within the fiber system. Differences in the path length between the interferometer arms led to constructive and destructive interference in the fibers and this caused the unwanted and dramatic fluctuations in the laser power. To fix this and suppress the interference, the fiber EOM was locked using a photo-detector and a Moku to create a feedback loop. A Moku is a digital instrument that can be configured as different instruments, like signal generators, mixers, and PID controllers, and used to create a feedback loop to frequency lock the laser.

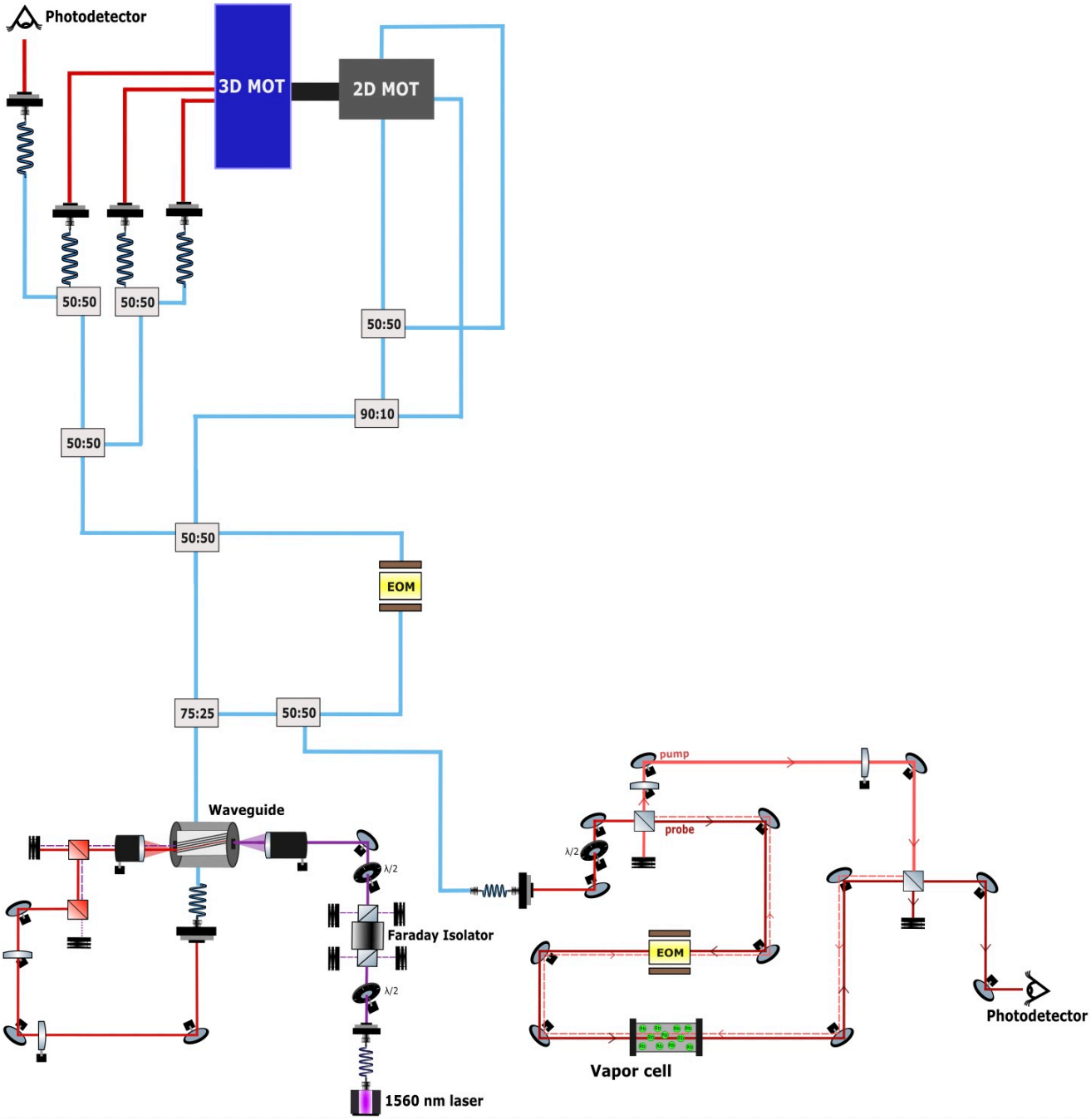

Figure 9: Complete beam path: SHG setup, vapor cell, fiber chain, 2D MOT, and 3D MOT

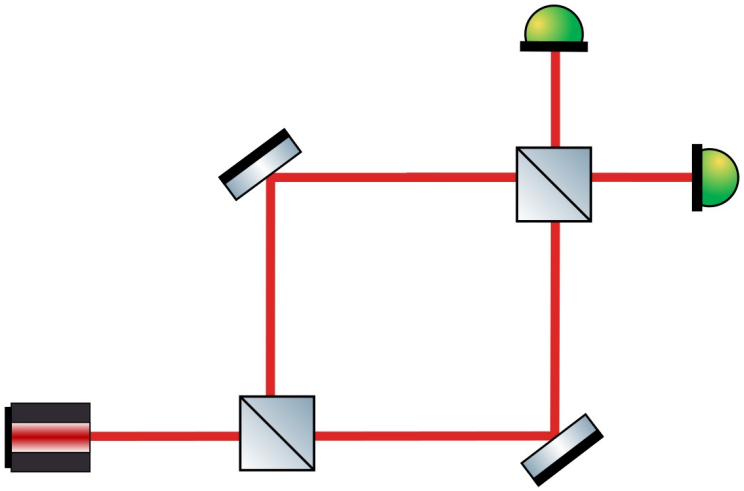

Figure 10: Mach Zehnder interferometer schematic

4.4 2D MOT

The function of the 2D MOT is to produce a cold atomic flux that can exceed 10^9 atoms per second [8]. Assembling the 2D MOT involved carefully attaching the printed circuit board (PCB) for the coil drivers and then putting together all the components as shown in Figure 11 and then attaching it to the vacuum chamber that housed the 3D MOT.

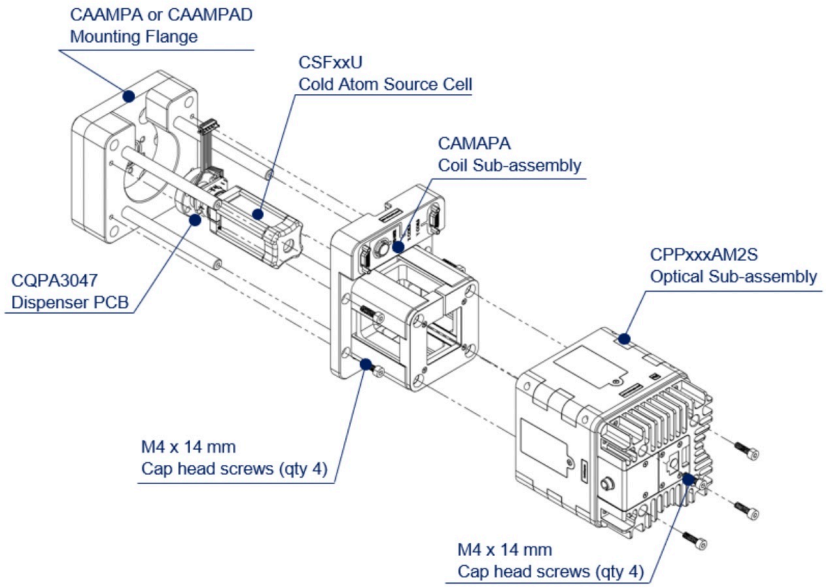

Figure 11: Diagram of the main components used in the 2D MOT [8]

Light for the 2D MOT was delivered through fiber optic cables that were connected to the chain of fibers described in the previous section. To confirm that the light was reaching the 2D MOT, beam profiling was performed. Figures 12a and 12b show the beam profiles visible on infrared viewer cards from the 2D MOT input fibers.

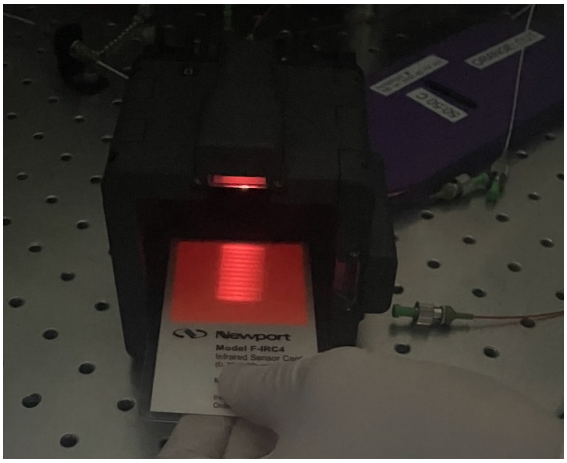

(a) Beam profile of one of the 2D MOT input beams.

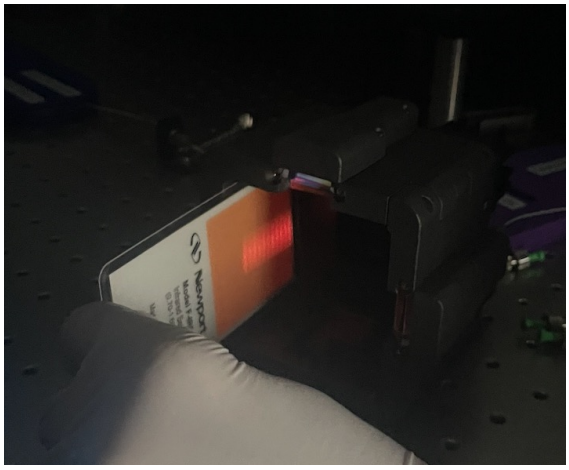

(b) Beam profile of an additional 2D MOT input beam.

Proper polarization was also essential for the 2D MOT to work efficiently. The polarization axis of each fiber output was aligned with the fiber key axis to ensure proper polarization. This was measured throughout the fiber network and individually at each 2D MOT fiber input.

If a steady stream of ^{87}Rb atoms were entering the 3D MOT, a bright fluorescence spot would appear at the center of Figure 13 below.

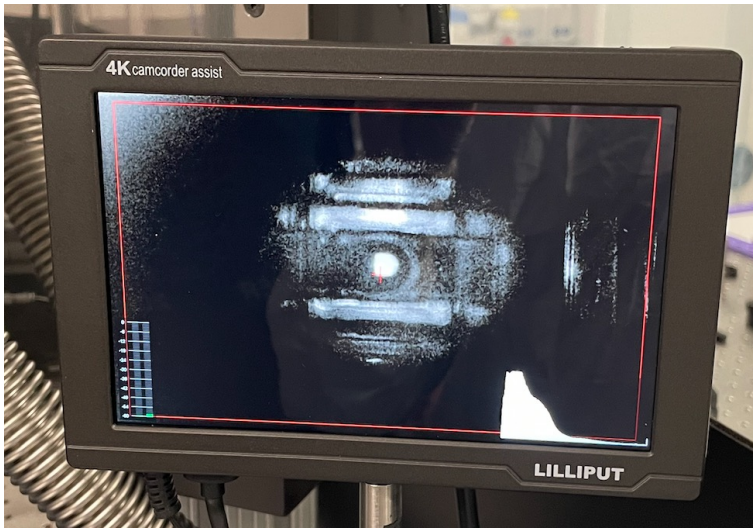

Figure 13: Image of the 2D MOT Rb cell region captured by the camera

While this was not observed, the camera image did show periodic haziness that would clear and then return as the laser power drifted when the EOM was unlocked. This was encouraging because it indicated that the laser frequency was sweeping across resonance, briefly exciting some of the ^{87}Rb atoms in the vapor cell causing them to fluoresce even though a continuous atomic beam was not yet produced. Additional troubleshooting will be required to achieve a stable atomic flux into the 3D MOT.

4.5 3D MOT

The 3D MOT was assembled to provide a stable platform for trapping and cooling atoms. The tabletop optics were assembled and placed; a diagram of the full layout, including labeled fiber beam splitters, is shown in Figure 9. Upstream of the MOT beams, a polarizing beam splitter (PBS) and half-wave plate (HWP) were added to clean and control the input polarization. The PBS produces a purely linear input, and the HWP sets its angle to achieve the desired circular polarization at the MOT beams.

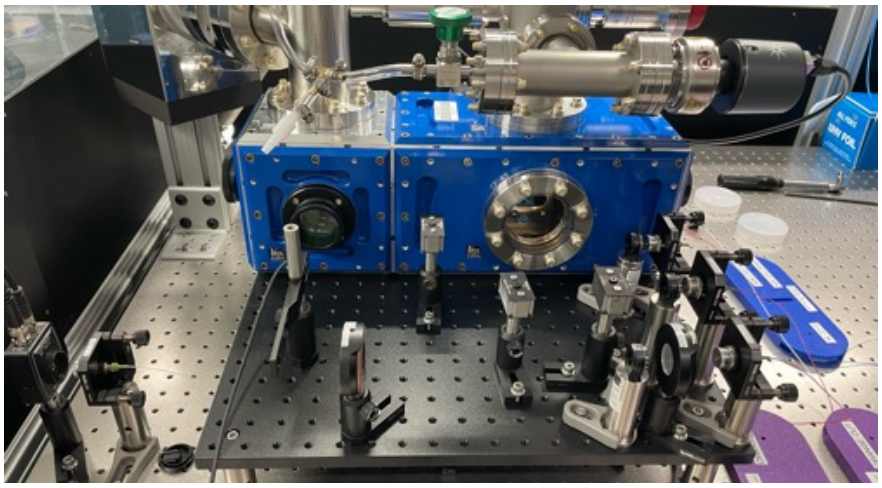

Figure 14: 3D MOT external optics

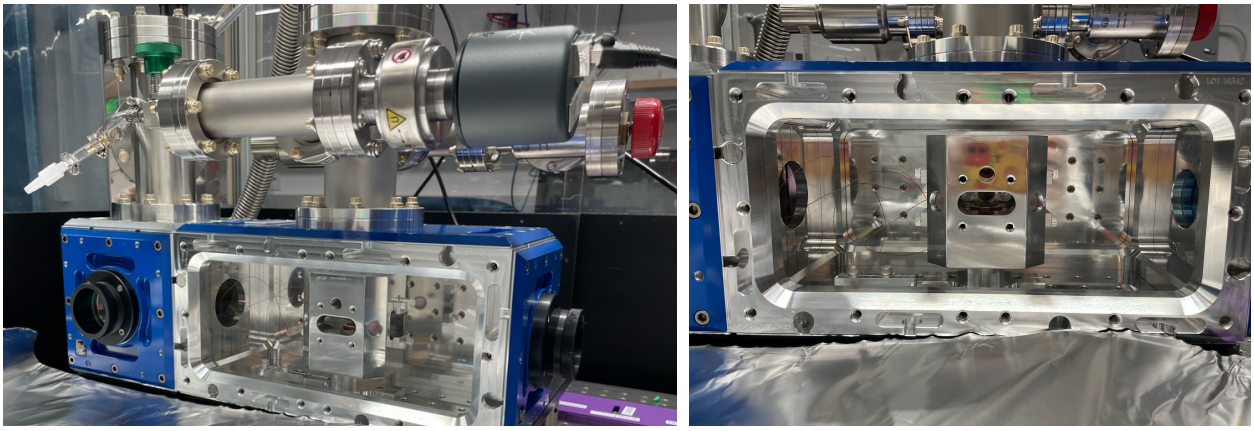

Figure 15: 3D MOT internal optics and magnetic coil holder inside of vacuum chamber

The internal optical components were then assembled and attached to the base. After screwing helicoils into the mount, three mirrors were placed in their slots and secured with rings. The remaining slots were filled with a waveplate and a mirror, each separated by a ring to avoid scratching the optics. Fiber collimators and MOT optics were assembled and placed in the chamber and adjusted so that the beams could overlap orthogonally in the MOT. The external optics were mounted to match the beam heights and magnetic coils were added in an anti-Helmholtz configuration to induce the quadrupole magnetic field gradient needed to trap atoms. Finally, the optics and coils were connected to the electronic systems.

5 Future Work

Once the 2D MOT reliably delivers a beam of Rb into the 3D MOT, the atoms will be cooled and trapped. Next steps will focus on characterizing the MOT to establish reliable operating settings. Brightness—which will indicate number of atoms in the atomic cloud—and cloud size will be measured and recorded using a camera. To gauge the velocity distribution, the cooling laser beams will be turned off and the rate at which the cloud spreads will be measured. The laser wavelength will be scanned to vary the detuning and the coil current configuration will be adjusted to see how these changes affect brightness, size, and stability of the atomic clouds.

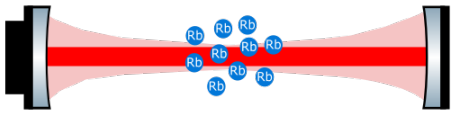

Figure 16: Atomic cloud in an optical cavity

The next stage of this project will focus on setting up an optical conveyor belt to transport the atoms away from the trap to be used as filters. The atoms must be transported away from the crowded MOT to a cleaner detection region with fewer MOT optics, less stray light, and reduced contamination from the Rb source. This is accomplished using a type of lattice transport which consists of two counter-propagating laser beams forming an optical dipole trap. When the beams have the same frequency, they create a standing wave with fixed nodes and anti-nodes resulting in a static trap. If one beam is slightly red-detuned, a traveling wave component is introduced which slowly shifts the position of the anti-nodes. The atoms are attracted to the intensity maxima of the laser and are transported adiabatically, preserving their quantum state in the optical dipole trap. Once moved to the detection region, the cold atom clouds can act as precise optical filters. Multiplexing is induced by spatial or temporal separation of the atom clouds along the optical conveyor belt and allows for multiple quantum states to be stored in superposition and read out simultaneously using techniques such as fluorescence or Raman transitions.

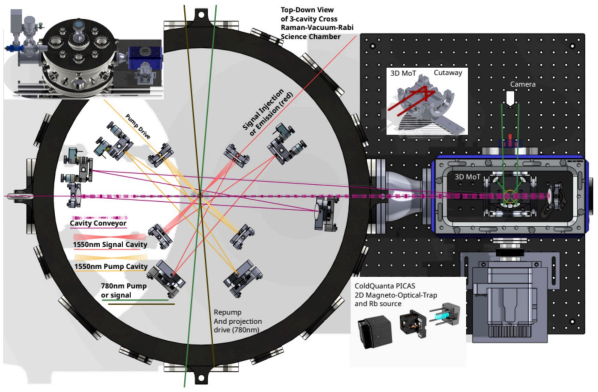

Figure 17: 3D MOT, optical conveyor belt, and science chamber

6 Acknowledgments

I would like to thank my mentors Daniel Grass and Lee McCuller, as well as all the members of the McCuller Lab—Jeffrey Wack, Torrey Cullen, Sander Vermeulen, Ian Macmillan, and Alex Ramirez. I would also like to thank the National Science Foundation and the Caltech LIGO SURF program for this amazing opportunity.

References

[1]LIGO Caltech, *What are gravitational waves?*, https://www.ligo.caltech.edu/page/what-are-gw, Accessed: 2025-05-13, n.d.

[2]S. M. Vermeulen, T. Cullen, D. Grass, I. A. O. MacMillan, A. J. Ramirez, J. Wack, B. Korzh, V. S. H. Lee, K. M. Zurek, C. Stoughton, and L. McCuller, "Photon-counting interferometry to detect geontropic space-time fluctuations with gquest", Phys. Rev. X **15**, 011034 (2025).

[3]L. McCuller, "Quantum optimal stochastic-signal searches: seeding "post-squeezing" — quantum metrology for fundamental physics", DOE QuantISED 2.0 Proposal for High Energy Physics, Submitted to DOE/SC Program Office SC-HEP, California Institute of Technology (2025).

[4]N. Hutzler, "Laser cooling and trapping", Physics 137a Lecture Notes (2024).

[5]R. W. Boyd, "Second-harmonic generation", Nonlinear Optics, 601 (2020).

[6]R. Paschotta, "Beat note", 10.61835/ua7"title="Thislinkwillreloadthecurrentpage. (2005).

[7]D. A. Steck, *Rubidium 87 d line data*, tech. rep. (Los Alamos National Laboratory, Theoretical Division (T-8), 2003).

[8]Infleqtion, Inc., *Infleqtion: quantum computing roadmap (picas)*, https://info.infleqtion.com/picas, Accessed: 2025-09-26, 2025.